Corkscrew point spread function for far-field three-dimensional nanoscale localization of pointlike objects

Matthew D. Lew,[1,2] Steven F. Lee,[2] Majid Badieirostami,[2] and W. E. Moerner[2,*]

[1]*Department of Electrical Engineering, Stanford University, 350 Serra Mall, Stanford, California 94305, USA*

[2]*Department of Chemistry, Stanford University, 375 North–South Axis, Stanford, California 94305, USA*

**Corresponding author: wmoerner@stanford.edu*

Received September 10, 2010; revised November 18, 2010; accepted December 10, 2010; posted December 14, 2010 (Doc. ID 134901); published January 11, 2011

We describe the corkscrew point spread function (PSF), which can localize objects in three dimensions throughout a 3.2 μm depth of field with nanometer precision. The corkscrew PSF rotates as a function of the axial (z) position of an emitter. Fisher information calculations show that the corkscrew PSF can achieve nanometer localization precision with limited numbers of photons. We demonstrate three-dimensional super-resolution microscopy with the corkscrew PSF by imaging beads on the surface of a triangular polydimethylsiloxane (PDMS) grating. With 99,000 photons detected, the corkscrew PSF achieves a localization precision of 2.7 nm in x, 2.1 nm in y, and 5.7 nm in z.

OCIS codes: 110.1758, 110.4850, 180.2520, 180.6900.

A plethora of scientific applications require nanoscale, noninvasive three-dimensional (3D) localization or tracking of objects from a distance. Fluorescence microscopy, in addition to satisfying these requirements, demonstrates the remarkable advantages of high sensitivity and label specificity. Unfortunately, the standard point spread function (PSF) of conventional microscopes is ill-suited for 3D localization. It contains very little information about the axial (z) location of an object near the focal plane [1–3], and it is symmetric above and below the focal plane. Recently, several methods have been developed to overcome these limitations for 3D localization, including introducing astigmatism to break the symmetry of the standard PSF [4–6], using mirrors to project the axial dimension onto a lateral dimension [7,8], imaging in multiple focal planes simultaneously [3,9–11], and interferometry [12,13].

Rotating PSFs, whose transverse intensity distributions rotate as they propagate, represent another class of methods for 3D microscopy, whereby the axial position of an emitter can be inferred from the angle of rotation of the PSF. Rotating PSFs are propagation-invariant optical fields composed of special superpositions of Gauss–Laguerre (GL) modes of the paraxial wave equation that form lines in the GL modal plane [14]. In this Letter, we detail the design of a new rotating PSF with a corkscrew shape, which forms a single helix as it propagates. We show that the corkscrew PSF can be used to determine the 3D position of an emitter throughout a 3.2 μm depth of field. The phase mask used to generate the corkscrew PSF and the PSF's GL modal composition are also discussed. Fisher information (FI) calculations indicate that the corkscrew PSF can achieve nanometer precision in all three dimensions with limited numbers of photons. Finally, 3D super-resolution microscopy with the corkscrew PSF is demonstrated by imaging fluorescent beads on a triangular polydimethylsiloxane (PDMS) grating.

In our experiments, the standard PSF of an inverted epifluorescence microscope (Olympus IX71, Japan) is convolved with the corkscrew PSF using a $4f$ optical processing section as in previous studies [15], except that the reflective phase-only spatial light modulator (SLM, Boulder Nonlinear Systems 512×512 XY Phase series, USA) in the Fourier plane is loaded with the phase mask corresponding to the corkscrew PSF. To demonstrate 3D imaging, we pumped 0.2 μm diameter fluorescent beads emitting at 645 nm (Invitrogen, carboxylate modified, USA) with a 641 nm laser (Coherent CUBE 640-100C, USA) and collected the fluorescence through a $100\times$ 1.4 NA oil-immersion objective (Olympus UPlanSApo $100\times/1.40$), dichroic beam splitter (Semrock Di01-R635-25 $\times$ 36, USA), and long-pass filter (Omega Optical 650AELP, USA). We used a piezoelectric objective lens positioner (Physik Instrumente PIFOC, Germany) to axially scan a sample of beads spin-coated on a glass coverslip. A drop of immersion oil ($n = 1.518$) was added to the top surface of the sample to prevent aberrations. The fluorescence was detected with an electron-multiplying charge-coupled Si camera (Andor iXon$^+$ DU-897, UK). As shown in Figs. 1(a) and 1(b), the corkscrew PSF smoothly rotates as a function of the axial (z) position of the emitter of interest and forms the shape of a corkscrew in 3D space, whose axis of rotation is centered at the transverse (xy) location of the emitter. In order to localize this axis, two images are sequentially collected for each object; the first uses the normal corkscrew PSF, and the second uses a version that has been rotated by 180°, performed by rotating the phase mask on the SLM. Consequently, the spot in the second image will be rotated 180° with respect to the corkscrew's axis of rotation; hence the center between the two spots is the xy location of the emitter. The angle of the line through the two spots relative to a reference line determines the z location of the emitter. Each spot was fitted to a symmetric Gaussian function in order to determine its position. We measured a calibration curve of the rotation angle versus z position [see Fig. 1(c)] by axially scanning a fluorescent bead in precise 50 nm steps.

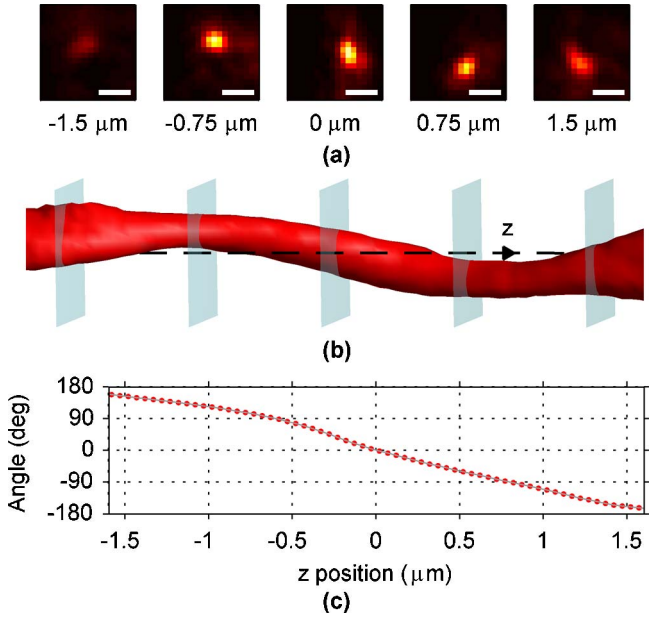

Fig. 1. (Color online) (a) Images of the corkscrew PSF collected from a fluorescent bead at various z positions. Scale bars are 1 μm. (b) 3D isosurface rendering of the corkscrew PSF, where the z positions of the blue planes correspond to the cross sections in (a). (c) Angle (extracted from pairs of images) versus z calibration curve measured at discrete z positions. The corkscrew PSF smoothly rotates 330 degrees over a 3.2 μm depth of field.

The corkscrew PSF is based upon a superposition of GL modes (m,n) [14] equal to (1,1), (2,4), (3,7), and (4,10). However, because these modes have both amplitude and phase components, convolving the fluorescence signal directly with these modes is highly photon-inefficient. Consequently, we designed an efficient phase-only mask to emulate the behavior of these modes. Following methods described previously [16], we optimized the corkscrew PSF's phase mask design by running an iterative optimization algorithm, using these modes as a starting point. This algorithm simultaneously enforced three constraints: (1) a phase-only mask in the Fourier plane of the $4f$ system; (2) a GL modal composition that is concentrated near the original superposition of modes described above; and (3) a Gaussian-like rotating spot in the image plane of the $4f$ system. The resulting phase mask and GL modal composition of the corkscrew PSF are shown in Fig. 2. Note that the cloud of GL modes surrounding the original superposition has the effect of limiting the rotation of the corkscrew PSF to a finite depth of field.

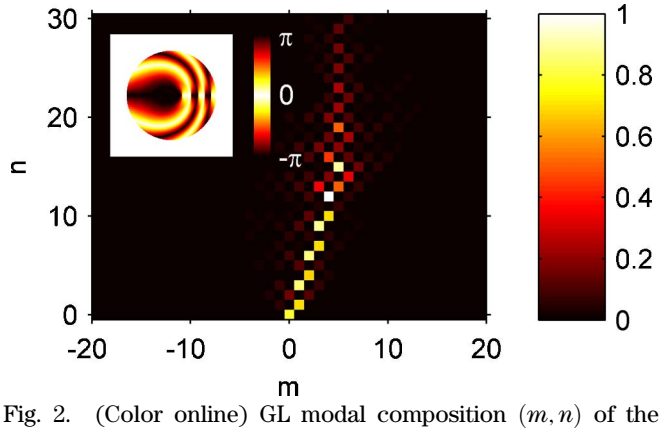

Fig. 2. (Color online) GL modal composition (m,n) of the corkscrew PSF in normalized units. Inset shows the corkscrew PSF phase mask in radians.

To quantitatively verify its 3D localization capabilities, we calculated the FI content of the corkscrew PSF. FI is useful when comparing different PSFs because the Cramér–Rao bound (CRB), which is the inverse of the FI matrix, gives the lower bound on the variance of any unbiased estimator. Thus, if the corkscrew PSF is used to measure 3D position, the CRB gives a lower bound on the localization precision, independent of the actual estimator used during any experiment. Following previously published methods [3,15], we calculated this limit, or the square root of the CRB, for the corkscrew PSF with 1000 photons detected and no extra noise. As shown in Fig. 3, the corkscrew PSF can achieve less than 10 nm precision in all three dimensions over a 3.2 μm depth of field. The localization precision of the corkscrew PSF is fairly flat over the center 2 μm depth of field and worsens gradually outside this range. The values in Fig. 3 are comparable to the localization precisions of the double helix PSF and other 3D methods [15,17,18]. The corkscrew PSF, however, can be used over a larger depth of field than other 3D methods; this advantage comes at the cost of imaging twice to determine rotation angle. These theoretical results demonstrate that the corkscrew PSF should be useful for photon-limited 3D localization applications.

We demonstrate 3D wide field super-resolution imaging with the corkscrew PSF by measuring the locations of fluorescent beads on a patterned PDMS surface, using an atomic force microscope tip characterization grating (MikroMasch TGG, Estonia) as a mold for the PDMS. To image the beads with the corkscrew PSF, the labeled surface was placed face down and optically coupled to a glass coverslip (Fisherfinest, No. 1 12-548-B, USA) with index-matched immersion oil. A white-light transmission image of the grating is shown in the inset of Fig. 4(a). The beads were illuminated with an intensity of 10 W/cm^2 and sequentially imaged using the original and rotated versions of the corkscrew PSF. A composite image of beads measured by the two PSFs is shown in Fig. 4(a). The locations of beads that settled in the lowest level "valleys" of the grating were used to measure and

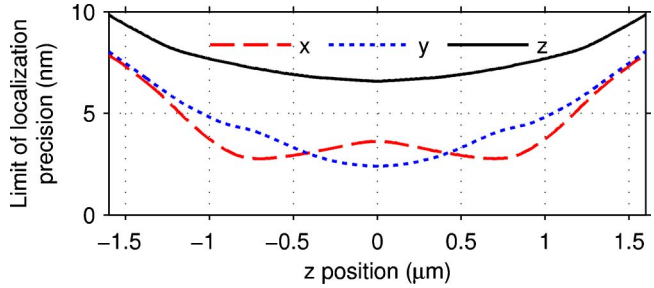

Fig. 3. (Color online) Limit of localization precision (square root of the CRB) attainable by the corkscrew PSF in x (red dashed curve), y (blue dotted curve), and z (black solid curve) for 1000 detected photons and no extra noise. Note the relatively uniform localization precision over the center 2 μm depth of field.

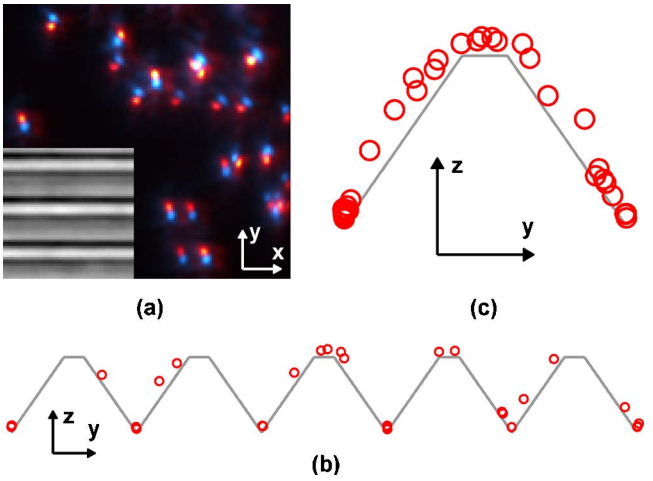

Fig. 4. (Color online) (a) Composite image of fluorescent beads on a triangular PDMS grating using the original (red) and rotated (cyan) versions of the corkscrew PSF. The height variations of the grating are clearly visible from the various orientations of the PSF. Inset shows a corresponding white-light image of the grating. The flat tops and large height of the grating, combined with tilted illumination, produce shadows in the image. Axis arrows are 3 μm. (b) Locations of beads (red circles, diameter = 0.2 μm) over multiple periods of the grating, projected onto the yz plane. Gray line is a model of the grating (3.0 μm periodicity, 1.8 μm height). Note the good agreement between bead locations and the grating model. Axis arrows are 1 μm. (c) Bead locations from multiple periods of the grating combined together, showing the translational symmetry of the measurement. Axis arrows are 1 μm.

compensate for the global tilt of the sample. In Fig. 4(b), the bead locations are projected along the axis of the grating (the x axis) and plotted as red circles matching the bead diameter. A model of the PDMS structure, based on the dimensions of the silicon grating, is also shown in Figs. 4(b) and 4(c). The bead locations exhibit good agreement with the model, especially when accounting for the possible roughness of the PDMS surface. Measurements over multiple periods of the grating are combined and plotted together in Fig. 4(c). This shows that the PDMS grating exhibits good periodicity over its lateral dimensions and that the corkscrew PSF can accurately localize objects throughout a large focal volume. During 34 measurements with a 100 ms exposure time, we achieved a localization precision, given as the standard deviation of the measured locations, of 2.7 nm in x, 2.1 nm in y, and 5.7 nm in z for a bead with an average of 99,000 photons detected per measurement (each consisting of two images). Because a large number of photons was detected, these measurements are most likely limited by the mechanical and thermal drift of the microscope stage.

In conclusion, the corkscrew PSF can localize objects in 3D space with nanoscale precision throughout a 3.2 μm depth of field using a conventional microscope, SLM, and 4f imaging system. FI calculations show that the corkscrew PSF can achieve nanometer localization precision in all three dimensions with limited numbers of photons. Furthermore, the PSF will also work with scattering objects. It is worth noting that sequential imaging can be avoided if two images are simultaneously recorded from two 4f sections, each containing a corkscrew mask, as in biplane imaging. This demonstrates that the corkscrew PSF is an excellent method for 3D wide field super-resolution microscopy.

We thank Michael Thompson, Quan Wang, and Dr. Randall Goldsmith for helpful technical discussions. This work was supported in part by grant R01GM085437 from the National Institute of General Medical Sciences. M. D. L. acknowledges support from a National Science Foundation (NSF) Graduate Research Fellowship and a 3Com Corporation Stanford Graduate Fellowship.

References

1. P. Prabhat, S. Ram, E. S. Ward, and R. J. Ober, IEEE Transactions on Nanobioscience **3**, 237 (2004).
2. A. Greengard, Y. Y. Schechner, and R. Piestun, Opt. Lett. **31**, 181 (2006).
3. S. Ram, P. Prabhat, J. Chao, E. S. Ward, and R. J. Ober, Biophys. J. **95**, 6025 (2008).
4. H. P. Kao and A. S. Verkman, Biophys. J. **67**, 1291 (1994).
5. L. Holtzer, T. Meckel, and T. Schmidt, Appl. Phys. Lett. **90**, 053902 (2007).
6. B. Huang, W. Wang, M. Bates, and X. Zhuang, Science **319**, 810 (2008).
7. M. D. McMahon, A. J. Berglund, P. Carmichael, J. J. McClelland, and J. A. Liddle, ACS Nano **3**, 609 (2009).
8. J. Tang, J. Akerboom, A. Vaziri, L. L. Looger, and C. V. Shank, Proc. Natl. Acad. Sci. USA **107**, 10068 (2010).
9. P. Prabhat, Z. Gan, J. Chao, S. Ram, C. Vaccaro, S. Gibbons, R. J. Ober, and E. S. Ward, Proc. Natl. Acad. Sci. USA **104**, 5889 (2007).
10. M. F. Juette, T. J. Gould, M. D. Lessard, M. J. Mlodzianoski, B. S. Nagpure, B. T. Bennett, S. T. Hess, and J. Bewersdorf, Nat. Meth. **5**, 527 (2008).
11. Y. Sun, J. D. McKenna, J. M. Murray, E. M. Ostap, and Y. E. Goldman, Nano Lett. **9**, 2676 (2009).
12. C. V. Middendorff, A. Egner, C. Geisler, S. W. Hell, and A. Schönle, Opt. Express **16**, 20774 (2008).
13. G. Shtengel, J. A. Galbraith, C. G. Galbraith, J. Lippincott-Schwartz, J. M. Gillette, S. Manley, R. Sougrat, C. M. Waterman, P. Kanchanawong, M. W. Davidson, R. D. Fetter, and H. F. Hess, Proc. Natl. Acad. Sci. USA **106**, 3125 (2009).
14. R. Piestun, Y. Y. Schechner, and J. Shamir, J. Opt. Soc. Am. A **17**, 294 (2000).
15. M. A. Thompson, M. D. Lew, M. Badieirostami, and W. E. Moerner, Nano Lett. **10**, 211 (2010).
16. S. R. P. Pavani and R. Piestun, Opt. Express **16**, 3484 (2008).
17. G. Grover, S. R. P. Pavani, and R. Piestun, Opt. Lett. **35**, 3306 (2010).
18. M. Badieirostami, M. D. Lew, M. A. Thompson, and W. E. Moerner, Appl. Phys. Lett. **97**, 161103 (2010).